A homozygous missense mutation in human *KLOTHO* causes severe tumoral calcinosis

Shoji Ichikawa,[1] Erik A. Imel,[1,2] Mary L. Kreiter,[3,4] Xijie Yu,[5] Donald S. Mackenzie,[1] Andrea H. Sorenson,[1] Regina Goetz,[6] Moosa Mohammadi,[6] Kenneth E. White,[5] and Michael J. Econs[1,5]

[1]Department of Medicine and [2]Department of Pediatrics, Indiana University School of Medicine, Indianapolis, Indiana, USA. [3]Division of Endocrinology, Children's Memorial Hospital, Chicago, Illinois, USA. [4]Department of Pediatrics, Feinberg School of Medicine, Northwestern University, Chicago, Illinois, USA. [5]Department of Medical and Molecular Genetics, Indiana University School of Medicine, Indianapolis, Indiana, USA. [6]Department of Pharmacology, New York University School of Medicine, New York, New York, USA.

Familial tumoral calcinosis is characterized by ectopic calcifications and hyperphosphatemia due to inactivating mutations in *FGF23* or UDP-*N*-acetyl-α-D-galactosamine:polypeptide *N*-acetylgalactosaminyltransferase 3 (*GALNT3*). Herein we report a homozygous missense mutation (H193R) in the KLOTHO (*KL*) gene of a 13-year-old girl who presented with severe tumoral calcinosis with dural and carotid artery calcifications. This patient exhibited defects in mineral ion homeostasis with marked hyperphosphatemia and hypercalcemia as well as elevated serum levels of parathyroid hormone and FGF23. Mapping of H193R mutation onto the crystal structure of myrosinase, a plant homolog of KL, revealed that this histidine residue was at the base of the deep catalytic cleft and mutation of this histidine to arginine should destabilize the putative glycosidase domain (KL1) of KL, thereby attenuating production of membrane-bound and secreted KL. Indeed, compared with wild-type KL, expression and secretion of H193R KL were markedly reduced in vitro, resulting in diminished ability of FGF23 to signal via its cognate FGF receptors. Taken together, our findings provide what we believe to be the first evidence that loss-of-function mutations in human *KL* impair FGF23 bioactivity, underscoring the essential role of KL in FGF23-mediated phosphate and vitamin D homeostasis in humans.

Introduction

Tumoral calcinosis (also referred to as hyperphosphatemic familial tumoral calcinosis, OMIM 211900) is a rare autosomal recessive metabolic disorder characterized by the development of often severe ectopic calcifications in soft tissues. Calcific masses are typically found around major joints such as the hip, elbow, shoulder, and knee. Biochemical abnormalities associated with tumoral calcinosis include hyperphosphatemia secondary to increased renal tubular phosphate reabsorption and elevated or inappropriately normal 1,25-dihydroxyvitamin D [1,25$(OH)_2$D] levels. Furthermore, this disorder is occasionally associated with diaphysitis, hyperostosis, arterial aneurysms, dental abnormalities, and angioid streaks of the retina.

Previous molecular genetic analyses demonstrated that tumoral calcinosis can result from biallelic inactivating mutations in genes encoding *FGF23* (1–4) or the UDP-*N*-acetyl-α-D-galactosamine:polypeptide *N*-acetylgalactosaminyltransferase 3 (*GALNT3*) (5–8). FGF23 is a hormone that promotes renal phosphate excretion by decreasing phosphate reabsorption in the proximal tubule and also reduces circulating 1,25$(OH)_2$D by both decreasing biosynthesis and increasing metabolism of 1,25$(OH)_2$D (9). GALNT3 is a Golgi-associated enzyme that initiates *O*-glycosylation of mature polypeptides. This enzyme selectively *O*-glycosylates a furin-like convertase recognition sequence in FGF23, thereby preventing proteolytic processing of FGF23 and allowing secretion of intact FGF23 (10). Therefore, dysfunction of either FGF23 or GALNT3 decreases circulating intact, bioactive FGF23, which leads to hyperphosphatemia and ultimately to tumoral calcinosis.

Recent studies have shown that FGF23 requires an additional cofactor, klotho (KL), to bind and signal through its cognate FGF receptors (FGFRs) (11, 12). Diminished *Kl* expression in mice results in a phenotype characterized by osteopenia, skin and muscle atrophy, pulmonary emphysema, infertility, hypoactivity, ectopic vascular and soft-tissue calcifications, and death by 60 days of age, which has been interpreted as a premature aging phenotype (13). Biochemical abnormalities of *Kl*-deficient mice include severe hyperphosphatemia, hypercalcemia, hypoglycemia, and increased serum levels of 1,25$(OH)_2$D (13–15). Of significance, the *Kl*-deficient phenotype largely overlaps with the phenotype of *Fgf23*-null mice (12, 16, 17), indicating functional crosstalk between KL and FGF23 and underscoring the observed direct interactions between KL, FGF23, and its cognate FGFRs (11, 12).

Herein we report a patient with severe vascular and soft-tissue calcifications as well as multiple abnormalities of mineral homeostasis due to a point mutation in the *KL* gene. Clinical and biochemical evaluation, together with functional studies, indicate that this mutation attenuates the ability of KL to support FGF23 signaling and causes deranged phosphate, vitamin D, and calcium homeostasis. To our knowledge, this is the first disease-causing mutation identified in the *KL* gene.

Results

Case report. A 13-year-old girl initially presented with complaints of fatigue and nightly frontal headaches without other neurological symptoms. She denied polyuria or polydipsia, and her past medical

Nonstandard abbreviations used: 1,25$(OH)_2$D, 1,25-dihydroxyvitamin D; EGR1, early growth response 1; FGFR, FGF receptor; GALNT3, UDP-*N*-acetyl-α-D-galactosamine:polypeptide *N*-acetylgalactosaminyltransferase 3; KL, klotho; PTH, parathyroid hormone.

Conflict of interest: The authors have declared that no conflict of interest exists.

Citation for this article: *J. Clin. Invest.* **117**:2684–2691 (2007). doi:10.1172/JCI31330.

Table 1
Laboratory data during the subject's clinical course

Parameter	Normal ranges	At presentation	After PTX	Prior to starting low PO_4 diet	While on low-PO_4 diet	After sevelamer treatment (2,400 mg TID)
Phosphorous (mg/dl)	3.0–4.5	6.4	7.9	7.8	7.4	6.9
Calcium (mg/dl)	8.8–10.8	12.1	10.4	9.9	10.2	10.1
Calcium-phosphorous product (mg^2/dl^2)		77	82	77	75	70
Creatinine (mg/dl)	0.3–1.1	0.7	0.5	0.5	0.5	0.6
Alkaline phosphatase (IU/l)	70–300	121		117	136	
Intact PTH (pg/ml)	15–55	121	11		61	56
25(OH)D (ng/ml)	20–60	20.7			14.6	25.9
$1,25(OH)_2D$ (pg/ml)	15–80	141.4			99.7	
Urine calcium (mg/dl)			2.7	<2.0		2.3
Urine creatinine (mg/dl)			55.7	79.3		89.5
Urine calcium/creatinine (mg/mg)	0.04–0.7	0.13	0.05			0.026
Urine 24-hour calcium (mg/kg/24 hours)		2.5				
TRP			98%			
Urine phosphorous (mg/dl)			16	42		24.8
C-terminal FGF23 (RU/ml)	72.9 ± 38.2			10,900		
Intact FGF23 (pg/ml)	29.7 ± 20.7			16,140		

Additional laboratory assessments included the following: normal complete blood count; IGF-1, 238.2 ng/ml (normal, 192–640 ng/ml); IGF binding protein-3, 2.7 mg/l (normal, 1.7–5.0 mg/l); prolactin, 13.7 ng/ml (normal, 2–17 ng/ml); fasting glucose, 70 mg/dl; fasting insulin, 8.19 μU/ml (normal, 2–17 μU/ml); total cholesterol, 150 mg/dl (normal, 112–208 mg/dl); HDL, 60.0 mg/dl (normal, 30–70 mg/dl); LDL, 74 mg/dl (normal, <100 mg/dl); and triglycerides 82 mg/dl (normal, 41–138 mg/dl). For FGF23, the normal mean ± SD is shown. PTX, parathyroidectomy; TRP, tubular reabsorption of phosphorous.

history was negative for fractures or kidney stones. Family history was negative for disorders of mineral metabolism as well as premature aging or premature death. On physical examination, height and weight were 149.2 cm (3rd–10th percentile) and 31.3 kg (<3rd percentile), respectively. Midparental height was 164 cm (50th percentile). She was normotensive, and general appearance was that of a normal pubertal girl without dysmorphic features or features of premature aging. Breast and pubic hair development were Tanner stage 3, and menarche subsequently developed normally. Dentition and musculoskeletal, neurological, and other system examinations were initially normal. However, she later developed mild swelling of the left lateral malleolus without erythema, warmth, or limitation of motion, and similar swelling also developed in the right thenar eminence.

Initial laboratory evaluation revealed markedly elevated serum calcium, phosphorous, $1,25(OH)_2D$, and parathyroid hormone (PTH) concentrations (Table 1). Dietary history indicated that vitamin and mineral intake was not excessive. Alkaline phosphatase and creatinine levels were normal. Although parathyroid ultrasound and scintigraphy suggested a single adenoma, 4-gland hyperplasia was found at surgery. Subtotal parathyroidectomy normalized her PTH and calcium. However, her calcium-phosphorous product remained elevated (Table 1). Tubular reabsorption of phosphorous was inappropriately high (98% of filtered phosphate) in the setting of hyperphosphatemia.

Skeletal radiographs revealed diffuse osteopenia; patchy sclerosis in the hands, feet, long bones and calvariae; intracranial calcifications (Figure 1A); as well as metacarpal periosteal reaction (Figure 1B). CT of the head demonstrated calcification of the dura and carotid arteries, without parenchymal calcifications (Figure 1C). Upon radiography, multiple punctuate calcifications were also visible in the Achilles tendon (Figure 1D). Renal ultrasound and echocardiogram were normal. Subsequent treatment with phosphate restriction (600–800 mg/day) and sevelamer (2,400 mg, 3 times a day) improved her serum phosphorous, although it remained elevated (6.9 mg/dl).

Serum FGF23 levels. Due to the biochemical and radiographic diagnosis of tumoral calcinosis, serum FGF23 levels in the patient were measured using 2 different ELISAs. FGF23 levels in our patient were 150- to 550-fold higher than the normal mean in both ELISAs. The intact FGF23 level was 16,140 pg/ml (normal mean, 29.7 ± 20.7 pg/ml; ref. 18), and the C-terminal FGF23 level (which includes both intact and C-terminal fragments) was 10,900 RU/ml (normal mean, 72.9 ± 38.2 RU/ml; ref. 18). In contrast, tumoral calcinosis patients with *FGF23* and *GALNT3* loss-of-function mutations have high C-terminal but low intact serum FGF23 levels (1, 4, 19, 20).

Mutational and structural analyses of KL. To identify the molecular defect associated with the observed clinical manifestations, mutational analyses were performed on candidate genes. The patient showed no disease-causing changes in the gene responsible for familial hypocalciuric hypercalcemia, the calcium sensing receptor (*CASR*), or the 2 genes previously associated with tumoral calcinosis, *FGF23* and *GALNT3*. Due to similarities in the biochemical phenotype between *Kl*-deficient mice and our patient, direct DNA sequencing of *KL* was performed and revealed that the patient had a homozygous A-to-G transition (c.578A>G) in exon 1 (Figure 2A). This nucleotide change was not found in 230 control white individuals by PCR-RFLP analysis with BsrI (data not shown), confirming the change to be a mutation.

This mutation replaced histidine 193 with arginine (H193R) in the first of the 2 tandem putative glycosidase domains, KL1. KL is alternatively spliced within exon 3 to produce membrane-bound and secreted KL forms. Thus, the H193R change, which maps to exon 1, was predicted to be present in both isoforms. H193 was fully conserved across species and across related family-1 glycosidases and their orthologs (Figure 2B). Structural analysis of myrosinase, a plant homolog of KL, revealed that this histidine

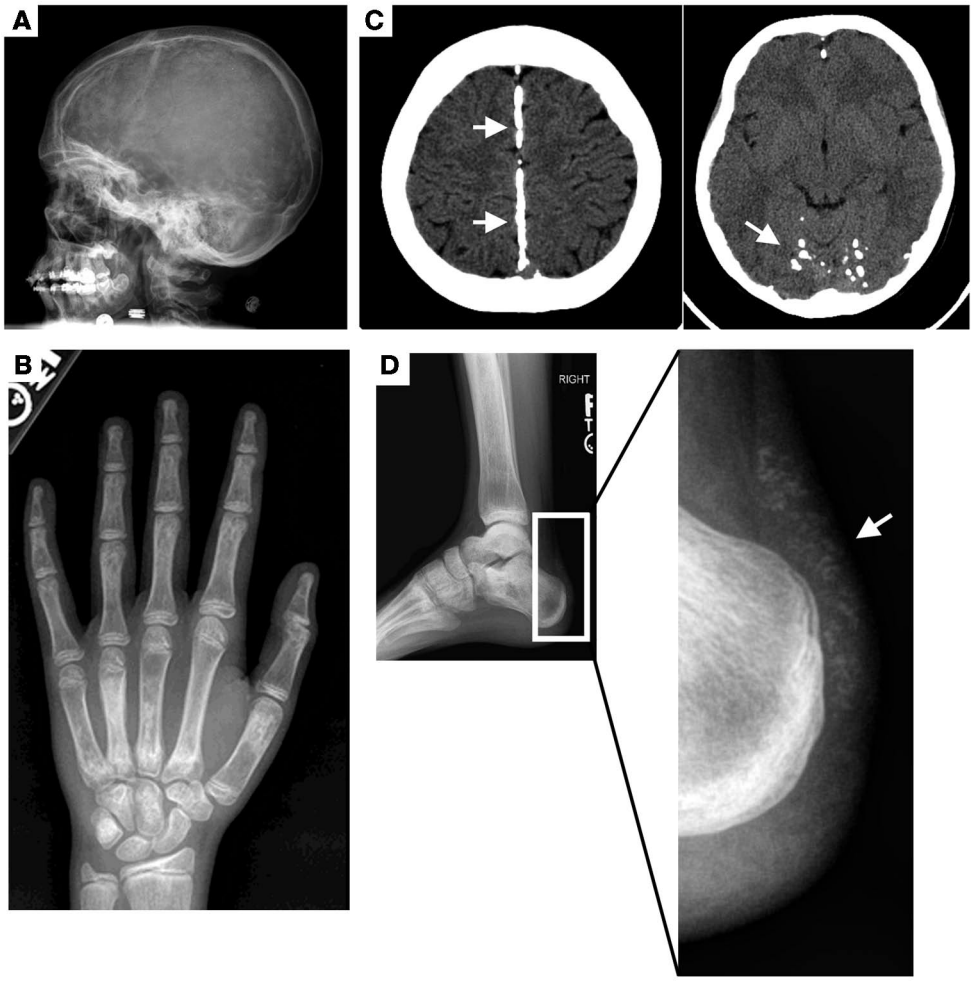

Figure 1
Radiographic imaging of the patient carrying the *KL* H193R mutation. (**A**) Intracranial calcification and short bulbous tooth roots. (**B**) Sclerosis in the left hand. (**C**) Head CT demonstrating midline areas of dural calcification and posterior fossa calcifications (arrows). (**D**) Plain radiograph of ankle with Achilles tendon calcifications (arrow).

residue was situated at the base of the deep catalytic pocket (Figure 2C). Replacement of the histidine with an arginine was predicted to introduce steric clashes with neighboring residues, and these spatial constraints should have destabilized the tertiary fold of the KL1 domain, leading to reduced expression and secretion of KL.

Analysis of KL protein expression. To test this hypothesis, we transiently expressed membrane-bound and secreted isoforms of wild-type and mutant KL in HEK293 cells. Compared with wild-type KL, total expression of the membrane-bound isoform was markedly reduced in mutant KL (Figure 3A). As previously demonstrated by others (11, 21), cells expressing wild-type KL produced 2 different species of membrane-bound KL. However, cells expressing the mutant KL had reduced or undetectable levels of fully glycosylated (mature) KL (Figure 3, A and B). Because of its location in the *KL* gene, the H193R mutation could also alter secreted KL protein. In this regard, there was prominent KL secretion from cells expressing wild-type KL, whereas almost no KL protein was detected in the media of cells expressing mutant KL (Figure 3A). However, when secreted KL was stably expressed for an extended period, minute amounts of mutant KL protein were detectable in the culture media of the cell line (data not shown). These data suggest that mutant KL is less stable than wild-type KL.

Since protein stability can often be improved by culturing cells at a lower temperature (22), we cultured cells stably expressing KL at 28.5°C and 37°C. Indeed, we found an increased expression of the mature mutant KL in cells cultured at lower temperature compared with cells maintained at 37°C, whereas the expression of wild-type KL was insensitive to changes in cell culture temperature (Figure 3B). These data are consistent with our structural prediction that the *KL* mutation reduces KL protein stability, manifesting in reduced protein expression and maturation.

FGF23 biological activity. KL is required for high affinity FGFR binding and bioactivity of FGF23 (11, 12). The effect of the H193R *KL* mutation on FGF23 biological activity was assessed by quantifying transcripts of the human early growth response 1 (*EGR1*) gene, a known downstream mediator of FGF23 signaling, in HEK293 cells (12). Stimulation of cells with FGF23 resulted in a 9-fold increase in *EGR1* mRNA in cells expressing wild-type KL, compared with control cells expressing vector alone (Figure 4). In contrast, consistent with reduced membrane-bound KL expression, FGF23-mediated *EGR1* expression was 6-fold lower in cells transfected with H193R KL ($P < 0.01$).

Coimmunoprecipitation analyses. To further investigate how the H193R mutation impairs the ability of KL to support FGF23 signaling, we studied the impact of the *KL* mutation on formation of the ternary FGF23-KL-FGFR1c complex. As shown in Figure 5 (top panel), FGF23 coprecipitated with wild-type KL but not with H193R KL. The *KL* mutation also affected the interaction between

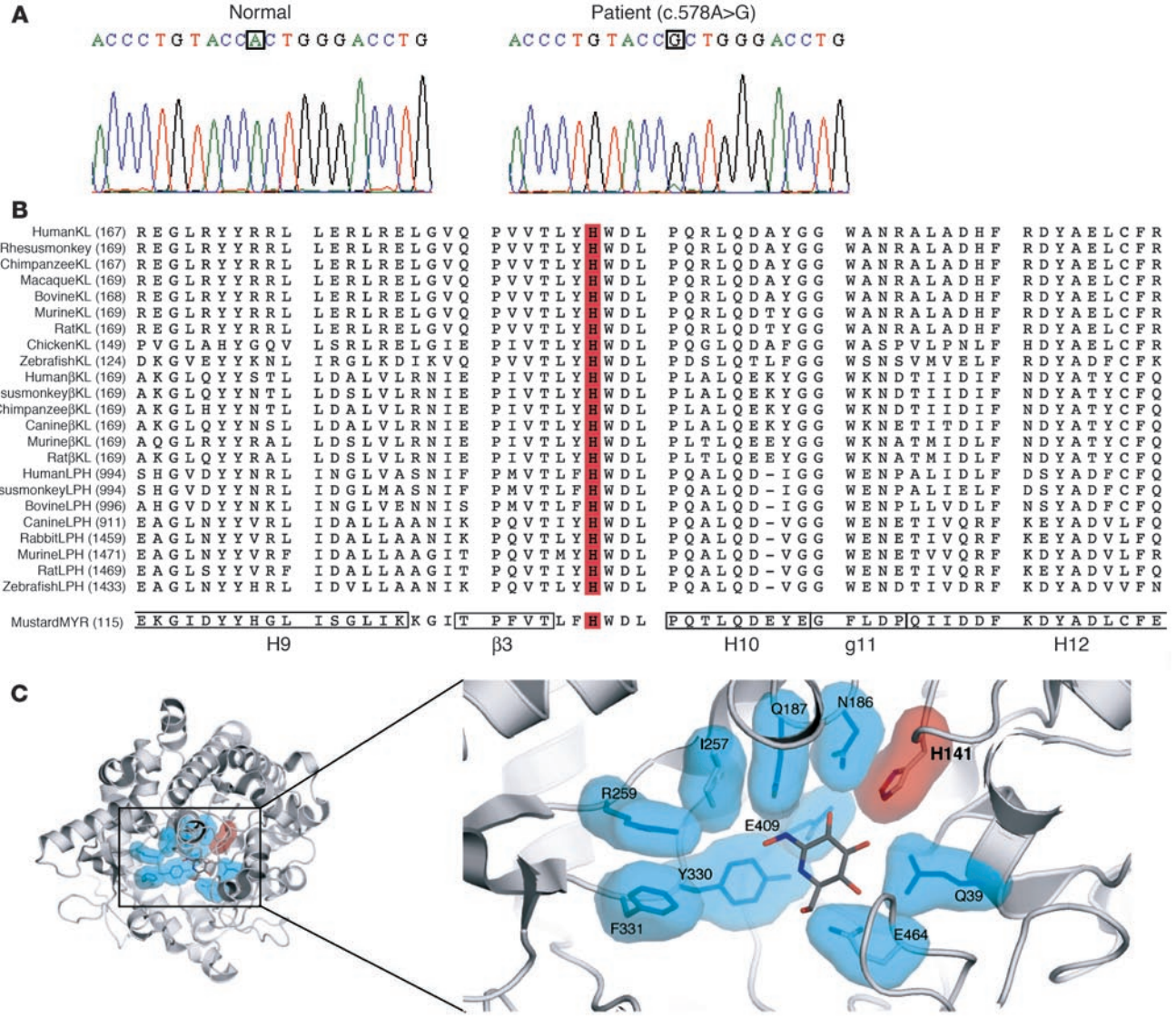

Figure 2
Mutational and structural analyses of the *KL* H193R mutation. (**A**) Mutational analysis of the *KL* gene. DNA sequencing of the *KL* exons revealed an A-to-G transition in exon 1 (boxes). Left, normal control; right, patient. c.578A>G, homozygous A-to-G transition. (**B**) Sequence alignment of the region encompassing the mutated histidine residue of KL and related family-1 glycosidases. LPH, lactase phlorizinhydrolase; MYR, myrosinase. Residue numbers are in parentheses to the left of the alignment. For myrosinase, secondary structure elements are denoted below the sequence, and the locations and lengths of the secondary structure elements are indicated by boxes in the sequence. H, α helix; β, β strand; g, g helix. A dash in the sequence represents a gap introduced to optimize the alignment. The histidine residue, which is mutated in KL of the patient presented in this study, is colored red. Note that this residue is conserved among family-1 glycosidases and their orthologs. (**C**) Ribbon representation of the crystal structure of myrosinase (Protein Data Bank [PDB] ID, 1E6S) and surface representation of catalytic site residues. White mustard myrosinase is a plant homolog of human KL. A close-up view of the catalytic cavity with bound substrate (gluco-hydroximolactam) is shown on the right, and to orient the reader, a view of the whole structure is shown on the left. Note that histidine 141 of the catalytic site is homologous to H193 of human KL.

KL and FGFR1c, although to a much lower extent than the effects on FGF23-KL binding. In complimentary experiments, KL was coprecipitated with FGF23, and the H193R mutation was found to markedly reduce KL coprecipitation with FGF23 (Figure 5, bottom panel). This reduced KL coprecipitation was consistent with low *EGR1* activation by FGF23 in the presence of mutant KL (Figure 4). The difference in binding between immunoprecipitations targeting epitopes in FGF23 and KL is likely due to the fact that precipitation with KL would pull down all mutant KL regardless of maturity and cellular location of the protein, whereas the precipitation with FGF23 would likely pull down only the mature KL on the cell surface, which appears to be the major species capable of interacting with FGFRs and FGF23 (11). In contrast, although FGF23 bound FGFR1c less efficiently with the H193R KL, FGFR1c still coprecipitated with FGF23 under these conditions (Figure 5, bottom panel). It should be noted, however, that FGFR1c was

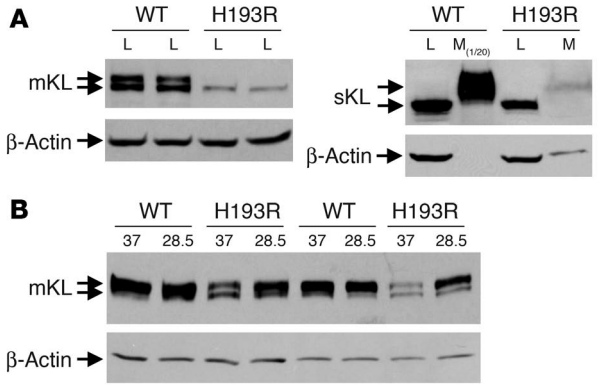

Figure 3
The *KL* mutation affects the total KL protein expression. (**A**) The *KL* mutation significantly reduces expression and secretion of KL. Wild-type and H193R KL isoforms were transiently expressed in HEK293 cells. Proteins in culture media (M) and cell lysates (L) were analyzed by immunoblotting with anti-V5 (KL) and β-actin antibodies. Only 1/20 volume of wild-type–secreted KL media ($M_{1/20}$; compared with H193R KL) was loaded on the gel. mKL, membrane-bound KL; sKL, secreted KL. (**B**) Temperature rescue of membrane KL expression. Cells stably expressing either wild-type or H193R membrane-bound KL were seeded equally and maintained in culture at either 37°C or 28.5°C. Expression of wild-type KL was comparable at the 2 temperatures tested, whereas increased amounts of fully glycosylated mutant KL protein was produced at the lower temperature in 2 independent experiments. All data are representative of at least 3 independent experiments.

overexpressed in the cells used for these studies, which may have masked the effect of the H193R mutation on the FGFR1c-KL interaction. FGFR1c also coprecipitated with FGF23 in the absence of KL (Figure 5, bottom panel). This observation is consistent with our previous surface plasmon resonance data showing that FGF23 can bind FGFR in vitro, albeit with low affinity (23).

Discussion

In this study, we identified what we believe to be the first disease-causing mutation in *KL*, H193R, in a patient presenting with severe tumoral calcinosis manifested by marked hyperphosphatemia with ectopic and vascular calcifications. The mutation drastically decreased protein expression of the membrane-bound and secreted forms of KL, which led to reduced FGF23-KL-FGFR1c complex formation on the cell surface and, ultimately, to impaired FGF23 signaling. Although substitution of H193 with arginine affects the tertiary fold of KL1 domain in KL, we cannot rule out the possibility that defective enzymatic activity of KL is implicated in impaired FGF23 signaling. Regardless, our data clearly show that KL dysfunction due to H193R mutation leads to a clinical phenotype reflecting impaired biological activity of FGF23.

Kl was originally described as a gene involved in aging, as *Kl*-deficient mice exhibited shortened lifespan and multiple aging-related phenotypes (13), whereas overexpression of the *Kl* gene in mice extended lifespan (24).Importantly, the phenotype of *Kl*-deficient mice closely parallels that of *Fgf23*-null mice (16, 17), indicating that KL and FGF23 have functions in the same metabolic pathway. Similar to mice deficient in *Kl* or *Fgf23*, our patient developed hypercalcemia, hyperphosphatemia, and increased $1,25(OH)_2D$ levels, resulting in ectopic calcifications and osteopenia. In contrast to *Kl*-deficient mice, however, our patient did not have a phenotype suggestive of abnormal or early aging. In addition, there was also no clinical evidence of emphysema, skin atrophy, delayed puberty (hypogonadotropic hypogonadism), or neural degeneration as was observed in the *Kl*-deficient mice. Likewise, tumoral calcinosis patients with *FGF23* or *GALNT3* mutations do not show signs of premature aging, although early dementia, most likely from cerebral calcifications, may occur (25). These observations, together with our present findings, support that KL likely serves as a factor controlling mineral ion homeostasis rather than aging. However, there are potential explanations for a lack of aging features in our patient. The *KL* mutation found in our patient did not result in complete loss of KL expression or secretion. Therefore, the patient retained partial KL function, as indicated in Figure 4. Possibly due to this partial activity of KL, the patient had not developed features of premature aging, although we cannot rule out that she may develop such features over time. It is also possible that humans are able to partially compensate for deficient KL function in a manner that lessens the effect on phosphate metabolism or other metabolic pathways, such that the phenotype may vary in severity and in details from the mouse model. Finally, this study demonstrated that the *KL* mutation impaired FGF23 signaling but it may not have affected other less well characterized functions of KL, which could be more relevant to premature aging.

Under normal physiological circumstances, hyperphosphatemia and FGF23 inhibit renal $1,25(OH)_2D$ synthesis, thereby leading to low $1,25(OH)_2D$ levels. However, compromised FGF23 signaling due to mutations in any of the 3 genes involved in tumoral calcinosis (*FGF23*, *GALNT3*, and now *KL*) disrupts this negative feedback mechanism, resulting in increased serum $1,25(OH)_2D$ concentrations and hyperphosphatemia (1, 4, 19, 20). In response to severe

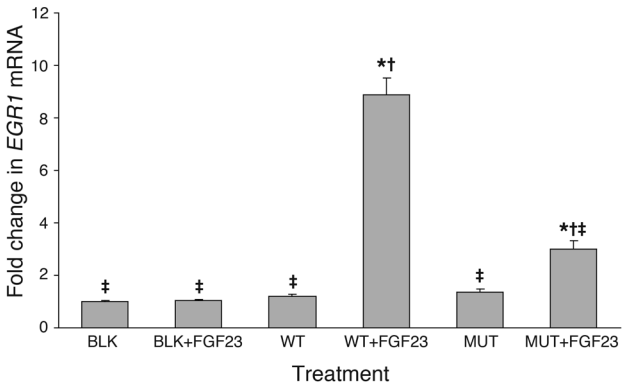

Figure 4
The *KL* mutation impairs KL-dependent FGF23 signaling. HEK293 cells were transiently transfected with vector alone (BLK), wild-type, or mutant (MUT) membrane-bound KL. The cells were treated for 30 minutes with 100 ng/ml FGF23 or vehicle. Relative *EGR1* mRNA expression was determined by real-time quantitative RT-PCR using β-*actin* as the internal standard (n = 6–8). Results are presented as fold change (mean ± SEM) compared to unstimulated cells. *P < 0.01, compared with BLK; †P < 0.01, compared with the same plasmid transfection without FGF23 treatment; ‡P < 0.01, compared with WT+FGF23.

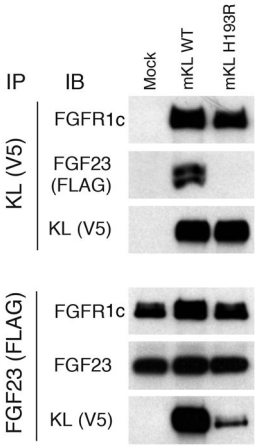

Figure 5
The *KL* mutation impairs the ability of membrane-bound KL to form a ternary complex with FGF23 and FGFR1c. HEK293 cells overexpressing wild-type or mutant mKL were transfected with FGFR1c and treated with FGF23. KL or FGF23 were immunoprecipitated, and the immunoprecipitates were analyzed for coprecipitated proteins by immunoblotting with the antibodies indicated.

hyperphosphatemia and increased $1,25(OH)_2D$ concentrations, our patient had appropriately elevated intact (functional) and C-terminal FGF23 levels. However, FGF23 signaling in our patient was severely compromised as a result of the diminished ability of mutant KL to form a ternary FGF23-KL-FGFR1c complex (Figure 5). In contrast, tumoral calcinosis patients with inactivating mutations in *FGF23* or *GALNT3* have highly elevated C-terminal fragments but low or undetectable levels of intact (active) FGF23 (1, 4, 19, 20). In these patients, FGF23 production is increased to compensate for hyperphosphatemia, but the FGF23 protein is unstable and readily cleaved by intracellular furin-like convertases, thereby preventing the necessary inhibition of renal phosphate reabsorption.

The disease severity of tumoral calcinosis is quite variable, ranging from solely eyelid calcifications (20) to massive periarticular calcifications (8, 19). Even considering the phenotypic variability of this disorder, our patient appeared to be more severely affected than previously reported cases. In this regard, the brain calcifications described herein have only been reported in 2 other patients with *GALNT3* mutations (in the choroid plexus [ref. 5] and dura [refs. 6, 26]). Furthermore, our patient had clinical features such as osteopenia and hypercalcemia that are seen in *Kl*-deficient mice (13, 27, 28) but have not been reported in previous tumoral calcinosis cases. Interestingly, both our patient and the *Kl*-deficient mouse have a combination of osteopenic and hyperostotic bones (13, 27, 28), similar to the hyperostotic lesions seen in a variant of tumoral calcinosis, hyperostosis-hyperphosphatemia syndrome. These differing clinical phenotypes most likely result from the different functional roles of the mutated genes.

Despite biochemical similarities such as high circulating levels of Fgf23 and hyperphosphatemia (12), there exist several biochemical differences between the *Kl*-deficient mice and our patient. First, although *Kl*-deficient mice have increased urinary calcium excretion (29), our patient did not have hypercalciuria. Second, *Kl*-deficient mice have abnormal regulation of insulin/IGF-1 signaling, resulting in hypoglycemia and increased insulin sensitivity. In contrast, our patient had normal fasting glucose and insulin concentrations. Third, PTH levels are low in the *Kl*-deficient mice when compared with wild-type mice (15) and similarly are predominantly low or normal in tumoral calcinosis cases that result from *FGF23* or *GALNT3* mutations. However, our patient had hyperparathyroidism at presentation and subsequently underwent subtotal parathyroidectomy of hyperplastic glands. The reason for the hyperparathyroidism was unclear, as elevated serum phosphate is a stimulus for PTH but high calcium and $1,25(OH)_2D$ inhibit PTH production. Since KL is expressed in the parathyroid glands (30), KL may have a direct role in the regulation of PTH in humans. Alternatively, this may be the result of tertiary hyperparathyroidism caused by persistent hyperphosphatemia. The lack of hyperparathyroidism in other tumoral calcinosis patients implies that this may be a feature limited to this particular patient. Further study of additional human cases will be required to clarify whether hyperparathyroidism is a unique response of our patient or a feature inherent to the disorder in humans.

In conclusion, we demonstrated that a homozygous loss-of-function *KL* mutation in a human resulted in severe tumoral calcinosis, not early aging as previously proposed. Despite the elevated circulating FGF23 concentrations, the H193R mutation diminished the ability of KL to function as a cofactor necessary for FGF23 signaling through FGFRs, leading to hyperphosphatemia, increased $1,25(OH)_2D$ concentrations, and subsequent ectopic calcifications. The fact that a mutation in *KL* was found in a patient with tumoral calcinosis demonstrates that, in addition to *FGF23* and *GALNT3*, *KL* should now be considered in the molecular diagnosis of tumoral calcinosis.

Methods

Patient and control individuals. The study was approved by the Institutional Review Board of Indiana University — Purdue University Indianapolis. Written informed consent was obtained from participants prior to participation in the study. Blood samples were collected from the patient with tumoral calcinosis and healthy race-matched individuals.

Measurement of serum biochemistries. Routine clinical biochemistries were analyzed by standard methods. FGF23 concentrations were determined using 2 different assays: FGF23 ELISA Kit (Kainos Laboratories Inc.), which recognizes only intact FGF23 with monoclonal antibodies, and Human FGF-23 (C-Term) ELISA Kit (Immutopics International), which detects both intact and C-terminal fragments of FGF23.

Mutational analyses. Genomic DNA was extracted from blood samples using the QIAamp DNA Blood Mini Kit (Qiagen). All exons and their adjacent intronic sequences for the *FGF23*, *GALNT3*, and *KL* genes were amplified using Taq DNA polymerase (New England Biolabs) or a Multiplex PCR Kit (Qiagen). Each PCR amplicon was directly sequenced from forward and/or reverse PCR primers using Big-Dye Terminator Cycle Sequencing Kit and the ABI PRISM 3100 Genetic Analyzer (Applied Biosystems). Mutational analysis for the calcium sensing receptor (*CASR*) gene was performed by GeneDx.

PCR-RFLP analysis of the A-to-G transition in *KL* was performed by amplifying genomic DNA harboring the transition, followed by restriction digest with BsrI (New England Biolabs). Forward and reverse PCR primers were 5′-AGACTCCCGGAACGCCAGT-3′ and 5′-GTGTCCAAGTGAAGCCTCGT-3′, respectively. The wild-type A allele produced 4 fragments (258, 230, 120, and 19 bp), whereas the G allele found in the patient produced 3 fragments (378, 230, and 19 bp) as the change disrupts 1 of the 3 BsrI restriction sites.

Computational analysis. Multiple sequence alignments were performed using Accelrys GCG software package (version 11.1.3). Structural analysis

of myrosinase was performed using O software program (version 11.0.4; http://xray.bmc.uu.se/~alwyn/).

Expression vectors. The membrane-bound and secreted forms of human *KL* cDNAs cloned into pcDNA3.1/V5-His expression vector (Invitrogen) were a generous gift from Harold Dietz (Howard Hughes Medical Institute, Johns Hopkins University, Baltimore, Maryland, USA). Mutant *KL*-H193R cDNA was generated using the QuikChange Site-Directed Mutagenesis Kit (Stratagene). Human *FGFR1c* was PCR amplified from hFGFR-1 (ATCC) and cloned into pcDNA3.1(+) expression vector (Invitrogen). Human *FGF23* mutant (R176Q) cloned into pFLAG-CMV-3 expression vector (Sigma-Aldrich) was described previously (31). All constructs were sequenced to verify introduction of the correct mutation and the absence of cloning artifacts.

HEK293 cell culture and transfection. HEK293 cells (ATCC) were cultured in DMEM/F-12 medium (Invitrogen) supplemented with 10% fetal bovine serum (HyClone; Thermo Fisher Scientific), 1% L-glutamine, 1% sodium pyruvate, and 1% penicillin-streptomycin at 37°C and 5% CO_2. Subconfluent cells were transiently transfected with wild-type KL or H193R KL plasmid DNAs, using Lipofectamine 2000 (Invitrogen). After transfection, the cells were maintained in culture for additional 48–96 hours before cell harvest and collection of conditioned media. For the generation of stable cell lines, cells were transfected with wild-type and H193R *KL* plasmid DNAs, reseeded into 20-cm dishes, and selected in medium containing 450 μg/ml Geneticin (Invitrogen) for 2 weeks. Neomycin-resistant monocolonies were picked for expansion. For temperature rescue experiments, cells of the stable KL cell lines were equally divided into two 60-mm plates and grown for 48 hours at either 37°C or 28.5°C.

Immunoblotting. Cell lysates and conditioned media were electrophoresed on 10% Tris-HCl Ready Gel precast gels (Bio-Rad) and blotted onto nitrocellulose membranes. Membranes were incubated with HRP-conjugated V5 antibody (Invitrogen). Immunoblots were developed with ECL Plus Western Blotting Detection Reagents (GE Healthcare).

Analysis of EGR1 gene expression. HEK293 cells (2×10^5 cells/well) were transiently transfected with 0.5 μg of plasmid DNA containing wild-type or mutant membrane-bound KL, using FuGENE 6 reagent (Roche Applied Science). Cells transfected with empty vector DNA served as a negative control. Transfected cells were starved with serum-free medium plus 0.2% BSA for 24 hours and then treated for 30 minutes with either vehicle (PBS) or 100 ng/ml FGF23 carrying R176Q and R179Q ADHR mutations. Total RNA was extracted from the cells using the RNeasy Mini kit (Qiagen). TaqMan primers and probes specific for human *EGR1* and β-*actin* mRNA were designed using Primer Express software (version 2.0; Applied Biosystems). *EGR1* and β-*actin* mRNA were amplified from 100 ng total RNA using the TaqMan Gold RT-PCR kit (Applied Biosystems) in the ABI-PRISM 7700 Sequence Detection System (Applied Biosystems). Relative gene expression was determined by analyzing the data using the $2^{-\Delta\Delta Ct}$ method (32). Statistical analysis was performed by paired Tukey-Kramer honestly significant difference (HSD) test using JMP Statistical Discovery Software 4.1 (SAS Inc.).

Immunoprecipitation. DNA encoding human FGFR1c was transfected into native HEK293 cells or HEK293 stably expressing either wild-type or mutant KL. After 48 hours, transfected cells were washed once with serum-free media and then incubated with conditioned media from cells secreting FLAG-tagged FGF23. Following a 2-hour incubation, the cells were washed and lysed with RIPA buffer (Sigma-Aldrich) containing protease inhibitors (Complete Mini Tablet; Roche Applied Science). Cell lysates were incubated overnight at 4°C with agarose beads carrying anti-FLAG or anti-V5 antibodies (Sigma-Aldrich). Agarose beads were washed, and immunoprecipitated proteins were analyzed by immunoblotting with antibodies against V5 (KL; Invitrogen), FLAG (FGF23; Sigma-Aldrich), FGFR1 (Cell Signaling Technology), or FGF23 (33).

Acknowledgments

We are indebted to the patient for her participation in this study. This work was supported by NIH grants R01 AR42228 (to M.J. Econs), DK63934 (to K.E. White), DE13686 (to M. Mohammadi), P01 AG18397, T32 AR07581, and T32 DK065549; the Irma T. Hirschl Trust (to M. Mohammadi); and funding from the Indiana Genomics Initiative (INGEN), which is supported in part by the Lilly Endowment Inc.

Received for publication December 22, 2006, and accepted in revised form May 25, 2007.

Address correspondence to: Michael J. Econs, Department of Medicine, Indiana University School of Medicine, 541 North Clinical Drive, Clinical Building 459, Indianapolis, Indiana 46202-5121, USA. Phone: (317) 274-1339; Fax: (317) 278-0658; E-mail: mecons@iupui.edu.

1. Araya, K., et al. 2005. A novel mutation in fibroblast growth factor 23 gene as a cause of tumoral calcinosis. *J. Clin. Endocrinol. Metab.* **90**:5523–5527.
2. Benet-Pages, A., Orlik, P., Strom, T.M., and Lorenz-Depiereux, B. 2005. An FGF23 missense mutation causes familial tumoral calcinosis with hyperphosphatemia. *Hum. Mol. Genet.* **14**:385–390.
3. Chefetz, I., et al. 2005. A novel homozygous missense mutation in FGF23 causes Familial Tumoral Calcinosis associated with disseminated visceral calcification. *Hum. Genet.* **118**:261–266.
4. Larsson, T., et al. 2005. A novel recessive mutation in fibroblast growth factor-23 causes familial tumoral calcinosis. *J. Clin. Endocrinol. Metab.* **90**:2424–2427.
5. Campagnoli, M.F., et al. 2006. Familial tumoral calcinosis and testicular microlithiasis associated with a new mutation of GALNT3 in a white family. *J. Clin. Pathol.* **59**:440–442.
6. Ichikawa, S., Lyles, K.W., and Econs, M.J. 2005. A novel GALNT3 mutation in a pseudoautosomal dominant form of tumoral calcinosis: evidence that the disorder is autosomal recessive. *J. Clin. Endocrinol. Metab.* **90**:2420–2423.
7. Specktor, P., Cooper, J.G., Indelman, M., and Sprecher, E. 2006. Hyperphosphatemic familial tumoral calcinosis caused by a mutation in GALNT3 in a European kindred. *J. Hum. Genet.* **51**:487–490.
8. Topaz, O., et al. 2004. Mutations in GALNT3, encoding a protein involved in O-linked glycosylation, cause familial tumoral calcinosis. *Nat. Genet.* **36**:579–581.
9. Imel, E.A., and Econs, M.J. 2005. Fibroblast growth factor 23: roles in health and disease. *J. Am. Soc. Nephrol.* **16**:2565–2575.
10. Kato, K., et al. 2006. Polypeptide GalNAc-transferase T3 and familial tumoral calcinosis. Secretion of fibroblast growth factor 23 requires O-glycosylation. *J. Biol. Chem.* **281**:18370–18377.
11. Kurosu, H., et al. 2006. Regulation of fibroblast growth factor-23 signaling by klotho. *J. Biol. Chem.* **281**:6120–6123.
12. Urakawa, I., et al. 2006. Klotho converts canonical FGF receptor into a specific receptor for FGF23. *Nature.* **444**:770–774.
13. Kuro-o, M., et al. 1997. Mutation of the mouse klotho gene leads to a syndrome resembling ageing. *Nature.* **390**:45–51.
14. Tsujikawa, H., Kurotaki, Y., Fujimori, T., Fukuda, K., and Nabeshima, Y. 2003. Klotho, a gene related to a syndrome resembling human premature aging, functions in a negative regulatory circuit of vitamin D endocrine system. *Mol. Endocrinol.* **17**:2393–2403.
15. Yoshida, T., Fujimori, T., and Nabeshima, Y. 2002. Mediation of unusually high concentrations of 1,25-dihydroxyvitamin D in homozygous klotho mutant mice by increased expression of renal 1alpha-hydroxylase gene. *Endocrinology.* **143**:683–689.
16. Shimada, T., et al. 2004. Targeted ablation of Fgf23 demonstrates an essential physiological role of FGF23 in phosphate and vitamin D metabolism. *J. Clin. Invest.* **113**:561–568. doi:10.1172/JCI200419081.
17. Sitara, D., et al. 2004. Homozygous ablation of fibroblast growth factor-23 results in hyperphosphatemia and impaired skeletogenesis, and reverses hypophosphatemia in Phex-deficient mice. *Matrix Biol.* **23**:421–432.
18. Imel, E.A., et al. 2006. Sensitivity of fibroblast growth factor 23 measurements in tumor-induced osteomalacia. *J. Clin. Endocrinol. Metab.* **91**:2055–2061.
19. Garringer, H.J., et al. 2006. The role of mutant UDP-N-acetyl-alpha-D-galactosamine-polypeptide N-acetylgalactosaminyltransferase 3 in regulating serum intact fibroblast growth factor 23 and matrix extracellular phosphoglycoprotein in heritable tumoral calcinosis. *J. Clin. Endocrinol. Metab.*

91:4037–4042.
20. Ichikawa, S., et al. 2006. Tumoral calcinosis presenting with eyelid calcifications due to novel missense mutations in the glycosyl transferase domain of the GALNT3 gene. *J. Clin. Endocrinol. Metab.* **91**:4472–4475.
21. Imura, A., et al. 2004. Secreted Klotho protein in sera and CSF: implication for post-translational cleavage in release of Klotho protein from cell membrane. *FEBS Lett.* **565**:143–147.
22. Larsson, T., et al. 2005. Fibroblast growth factor-23 mutants causing familial tumoral calcinosis are differentially processed. *Endocrinology.* **146**:3883–3891.
23. Yu, X., et al. 2005. Analysis of the biochemical mechanisms for the endocrine actions of fibroblast growth factor-23. *Endocrinology.* **146**:4647–4656.
24. Kurosu, H., et al. 2005. Suppression of aging in mice by the hormone Klotho. *Science.* **309**:1829–1833.
25. Beck, D.A., Gray, L., and Lyles, K.W. 1998. Dementia associated with hyperphosphatemic tumoral calcinosis. *Clin. Neurol. Neurosurg.* **100**:121–125.
26. Martinez, S., Vogler, J.B., 3rd, Harrelson, J.M., and Lyles, K.W. 1990. Imaging of tumoral calcinosis: new observations. *Radiology.* **174**:215–222.
27. Kawaguchi, H., Manabe, N., Chikuda, H., Nakamura, K., and Kuro-o, M. 2000. Cellular and molecular mechanism of low-turnover osteopenia in the klotho-deficient mouse. *Cell. Mol. Life Sci.* **57**:731–737.
28. Yamashita, T., Okada, S., Higashio, K., Nabeshima, Y., and Noda, M. 2002. Double mutations in klotho and osteoprotegerin gene loci rescued osteopetrotic phenotype. *Endocrinology.* **143**:4711–4717.
29. Tsuruoka, S., et al. 2006. Defect in parathyroid-hormone-induced luminal calcium absorption in connecting tubules of Klotho mice. *Nephrol. Dial. Transplant.* **21**:2762–2767.
30. Takeshita, K., et al. 2004. Sinoatrial node dysfunction and early unexpected death of mice with a defect of klotho gene expression. *Circulation.* **109**:1776–1782.
31. White, K.E., et al. 2001. Autosomal-dominant hypophosphatemic rickets (ADHR) mutations stabilize FGF-23. *Kidney Int.* **60**:2079–2086.
32. Livak, K.J., and Schmittgen, T.D. 2001. Analysis of relative gene expression data using real-time quantitative PCR and the $2^{-\Delta\Delta CT}$ method. *Methods.* **25**:402–408.
33. White, K.E., et al. 2001. The autosomal dominant hypophosphatemic rickets (ADHR) gene is a secreted polypeptide overexpressed by tumors that cause phosphate wasting. *J. Clin. Endocrinol. Metab.* **86**:497–500.